Journal of the European Ceramic Society **15** (1995) 425–434

0955-2219/95/$9.50

0955-2219(95)00013-5

Room Temperature Tensile and Flexural Strength of Ceramics in AlN–SiC System

Houssam A. Toutanji,[a] David Friel, Tahar El-Korchi,[b] R. Nathan Katz, Gary Wechsler[c] & William Rafaniello[d]

[a]University of Puerto Rico, Mayaguez, PR 00681, Puerto Rico
[b]Worcester Polytechnic Institute, Worcester, MA 01609, USA
[c]Army Materials Laboratory, Watertown, MA 02172, USA
[d]Dow Chemical Co., Midland, MI 48674, USA

(Received 12 September 1994; revised version received 12 December 1994; accepted 10 January 1995)

Abstract

Tensile and bend strength were obtained for four compositions in the aluminum nitride–silicon carbide system: AlN, 75%AlN–25%SiC particulate, 50%AlN–50%SiC solid solution and SiC. Room temperature tensile strength, four-point bend strength, and the Weibull parameters for each of the tested materials are presented. Optical and SEM fractography were employed to identify failure initiating flaws for the fractured tensile specimens. The four-point bend strength is predicted using the Weibull tensile parameters and compared to measured values. Accuracy of the predicted results are rationalized based on observed microstructures and failure initiating flaws.

Introduction

Advanced ceramics are being increasingly utilized in a wide variety of demanding structural and electronic applications.[1] The high elastic modulus, excellent wear behavior, low density, high thermal conductivity, and outstanding high temperature strength and oxidation resistance of SiC have led to its use in wear parts, heat exchangers, fixturing for semiconductor manufacturing processes, and armor. AlN has outstanding thermal conductivity and a thermal expansion coefficient near that of silicon. These properties have made AlN the material of choice in electronic packages where heat management is a dominant design issue. However, because of its relatively modest strength and poor oxidation characteristics, except for use in armor systems, AlN receives little consideration in structural applications.

The AlN–SiC binary is somewhat unique among covalent systems in as much as a range of composites and solid solutions are possible depending on the raw materials and the processing conditions employed. If fine powders are processed significantly above 2100°C, a nearly complete range of solid solutions are possible.[2] Alternatively, if coarser materials are processed below 2000°C, where diffusion is slow, a family of two-phase particulate composites are formed.[3] While the mechanical properties of the end members, SiC[4–6] and AlN,[7–10] have been well documented, there have been only limited results reported for AlN–SiC composites and solid solution. Flexural strength data for AlN–SiC solid solutions were first reported by Ruh and Zangvil.[11] The low reported values were attributed to poor mixing. Landon and Thevenot using improved slurry preparation routes formed largely AlN–SiC solid solutions.[12] In general, the strength was higher for the SiC rich compositions. The maximum RT 3-point bend strength was reported as 1000 MPa for a hot pressed AlN–SiC material containing 25 wt% AlN. More recently, researchers at Nagoya University studied the effect of different microstructures on the mechanical properties of a single 30/70 AlN–SiC composition.[13] RT 4-point bend tests of this material demonstrated strengths and Weibull moduli increasing from 589 to 674 MPa and from 7·6 to 10·5 MPa, for the as processed solid solution and a phase separated modulated structure, respectively.[14] Mariano, *et al.*[15] have recently reported limited data on the RT 4-point bend strength of 15 and 45% SiC particulate reinforced AlN composites. They reported strengths of 477 and 347 MPa, respectively.

This work presents a detailed examination of the room temperature tensile and flexural strengths, failure statistics, and strength limiting flaws for four representative materials in the AlN–SiC system. The two end members, one solid solution alloy (50/50), and one particulate strengthened

composite (75/25) were studied. The solid solution and composite were selected based on their performance as ceramic armor materials[16] and potential for other structural applications.

Experimental Procedure

Materials

All of the specimens used in this study were machined from large billets. AlN, the AlN–SiC composite, and the AlN–SiC solid solution were prepared by hot-pressing blocks which were 38 × 104 × 20–40 mm thick in graphite dies. The three hot-pressed materials were pressed at 34·5 MPa and no sintering aids were employed. The exact processing conditions and physical characteristics of these compositions and the pressureless sintered SiC are provided in Table 1. The SiC parts were prepared using the traditional sintering aids of boron and carbon. The sintered dimensions for the SiC tiles were 112 × 112 × 16 mm. Both flexure and tensile specimens were machined out of each billet. The tensile test specimens were cylindrical rods measuring between 103 and 112 mm in length and 9–9·2 mm in diameter. B type bend bars, 3 × 4 × 40 mm, were prepared according to MIL-STD-1942A.[17]

Typical microstructures of the four ceramics studied are shown in Fig. 1. AlN and the 50/50 AlN–SiC solid solutions have uniform, fine-grained microstructures. Despite a processing temperature nearly 500°C higher than AlN, the average grain size was almost a factor of 4 smaller for the solid solution (see Table 1). The TEM micrograph, Fig. 2, of the 50/50 alloy vividly shows this fine grain size. The SiC microstructure is characteristic of other beta SiC materials having transformation induced large (50 × 2 mm) needle-like grains interspersed in a relatively fine microstructure (2 mm). From the optical micrographs, the 75/25 AlN–SiC composite appears to have fine SiC particles uniformly dispersed in an AlN matrix. However, TEM examination revealed that some dissolution of SiC into the AlN matrix grains had occurred. From EDS analysis of individual matrix grains, as much as 8% SiC was present in the AlN.[18]

Mechanical testing

Tensile tests were performed at room temperature utilizing a self-aligning hydraulic technique developed by Baratta and Driscoll[19,20] with a simplified specimen described by Hermansson, *et al.*[21] The tensile test specimens are cylindrical bars measuring between 103 and 112 mm in length and 9·0–9·2 mm in diameter. Forty mm on each end of the ceramic rod is inserted into a steel piston and adhesively bonded in place with a high strength epoxy.[22,23] The specimen–piston assembly is inserted into the pressure chamber of the hydraulic tester.* The pressure is applied and increased until the specimen is broken apart by the hydraulic pressure acting against the pistons. The pressure chamber, with specimen inserted, is shown schematically in Fig. 3. The internal pressurization of the specimen suspended between the O-ring seals minimizes bending stresses. The nominal tensile fracture stress (uncorrected for eccentricity) may be calculated by using the hydraulic pressure at failure and geometric parameters of the specimen–piston assembly.[20] A small degree of triaxiality in the hydrostatic loading of the specimen exists causing a small deviation from the uniaxial stress state, calculated to be less than 5%.[23,24] In addition, to eliminate the effects of stress intensification at the rod to piston bond transition, data from specimens that fractured within one half the radius of the specimen from the piston glue line are not used. Fractures occurring in these locations are considered invalid tests.[21]

Although this tensile method is inherently self-aligning, a small degree of eccentricity or misalignment of the tensile specimens can still occur from two sources. The specimen can be slightly curved or can be glued off-center in the pistons.

*ASCERA Hydraulic Tensile Tester, Robertsfors, Sweden.

Table 1. Processing conditions and physical characteristics

	AlN Hot pressed	*75AlN–25SiC Hot pressed (particulate reinforced)*	*50AlN–50SiC Hot pressed (solid solution)*	*SiC Sintered*
Hot pressing/ sintering temp.°C	1750	2000	2300	2120
Atmosphere	N_2	N_2	N_2	Ar
Density g/cm^3 (%TD)	3·26 (99·9)	3·24 (99·7)	3·22 (99·6)	3·17 (98·8)
Grain size (μm)	1·9 ± 0·6	AlN ≈ 2 μm SiC ≈ 5 μm	0·5 ± 0·2	Bimodal, 2·0 ± 0·6 and 50 × 2 plates
Phases (XRD)	2H AlN very slight AlON	2H AlN (solid sol'n) 3C-SiC	2H (solid sol'n)	3C, 6H minor-other polytypes

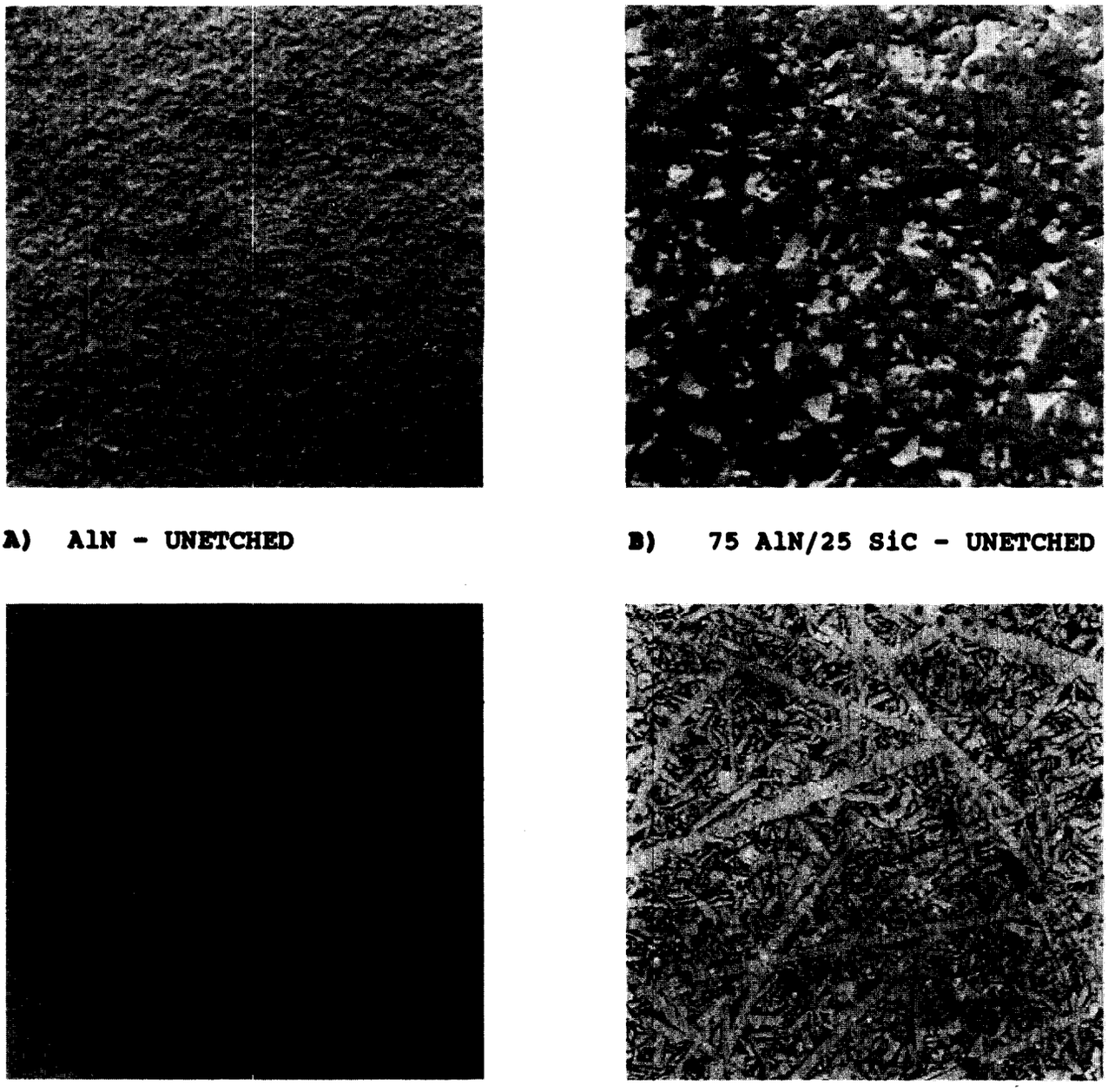

Fig. 1. Optical micrographs AlN–SiC system (original magnification 1000×).

As a result, small bending moments may develop along the gage length. The procedures to correct for this error have been described,[22–25] and were applied to the data reported in this paper.

The stress is related to the hydraulic pressure and test geometry by the following expression:

$$\sigma = \sigma_{nom} + \Delta\sigma = \left(\frac{A - A_s}{A_s}\right) \times P + \Delta\sigma$$

Where: σ_{nom} is the nominal (uncorrected) fracture stress, A is the cross-sectional area of the piston, A_s is the cross sectional area of the specimen, P is the pressure at failure, and $\Delta\sigma$ is the correction for eccentricity which is equal to $\sigma_{nom} \times f$(fracture origin location, specimen eccentricity and diameter).[22–25] The maximum correction for eccentricity in this study was equal to 8·40% with an average correction being approximately 4%.

Four-point bend tests were carried out in accordance with the MIL-STD-1942A standard test.[17] B type bend bars were used, having a size of 3 × 4 × 40 mm with 40 mm outer and 20 mm inner spans as shown in Fig. 4. Tests were carried out on an Instron 4201 universal tensile testing machine.

The fracture surfaces of the tensile specimens were examined by both low magnification optical and high magnification scanning electron microscopy (SEM). SEM fractography and elemental analysis were carried out on a JEOL 840A instrument equipped with an energy dispersive analyzer. The tensile fracture surfaces were ultrasonically cleaned and coated with thin layer of Au–Pd alloy

Fig. 2. TEM of 50/50 solid solution alloy of SiC/AlN showing the sub-micron grain size, ≈ 1/2 μm.

to prevent charging in the SEM. The bend bars shattered into many fragments upon fracture. This made it difficult to do unambiguous fractographic analysis and determine the location of fracture initiation of the bend bars. Consequently, such data will not be reported.

Results and Discussion

Tensile tests

Weibull distributions for the tensile strength of all

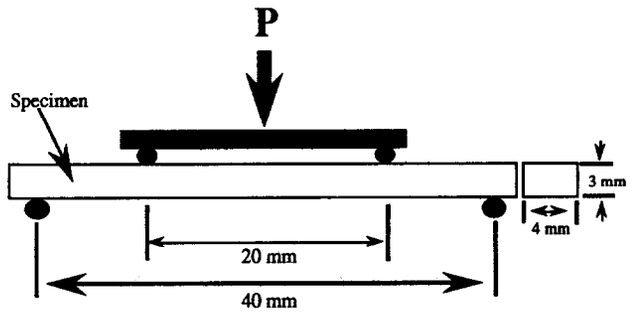

Fig. 4. Four-point bend test.

materials were plotted using the maximum likelihood estimate and are shown in Fig. 5. The characteristic tensile strength of 75%AlN–25%SiC and 50%AlN–50%SiC materials were higher than either of the base materials with values of 371 and 361 MPa, respectively. The AlN material was the weakest among the four materials with a characteristic strength of 234 MPa. The 50%AlN–50%SiC solid solution had the lowest scatter in strength with a Weibull modulus of 26·4. This may be attributed to the uniform nature of this material's microstructure. The other three materials (AlN, SiC, and 75%AlN–25%SiC) all had comparable scatter with Weibull moduli ranging between 9·1 and 12·7, as shown in Fig. 5. The summation of the effective volumes under stress for each set of materials tested is also reported in Fig. 5. 80% of the tested specimens produced valid breaks, 43 out of 53. Details on the tested specimens and the location of the fracture initiating flaws for each material are presented in Table 2.

Fractography of the tensile bars

Low magnification optical fractographs of a typical tensile specimen failure of each of the four materials are presented in Fig. 6, and higher magnification SEM's are presented in Figs 7–11. The AlN samples typically exhibit a well defined

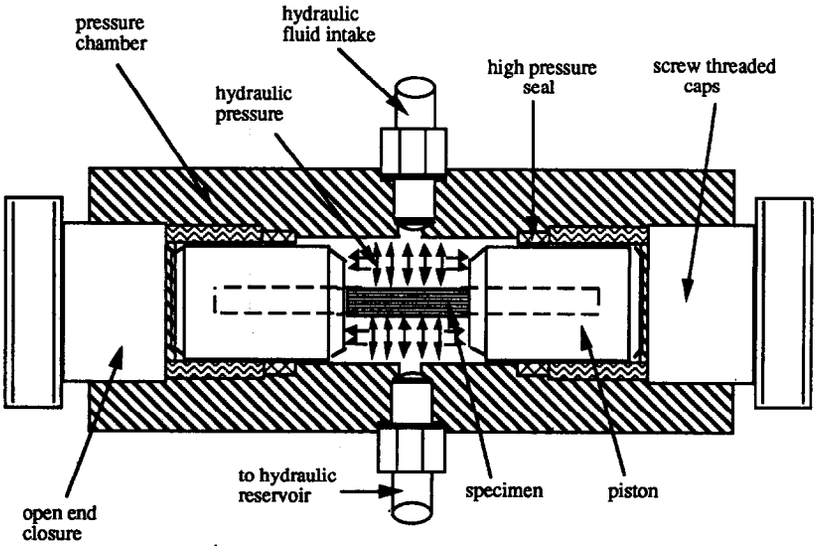

Fig. 3. Hydraulic pressure chamber with specimen–piston assembly.

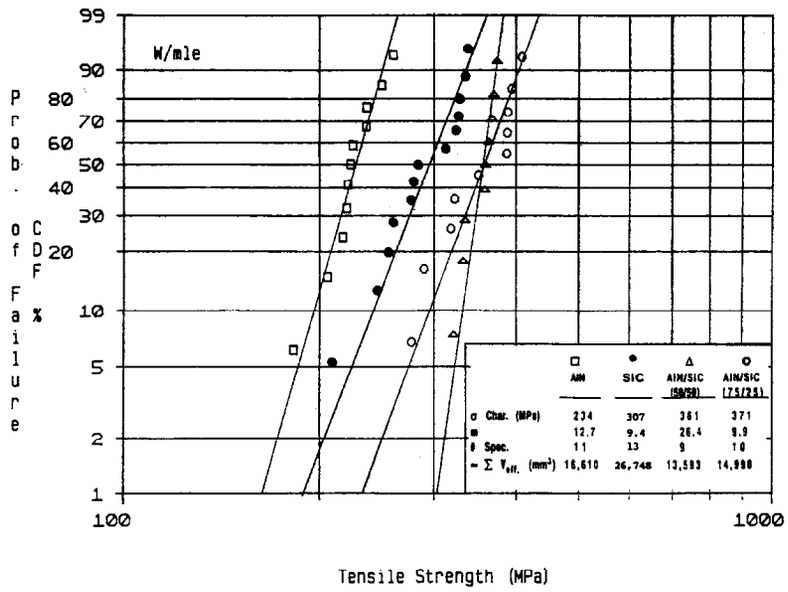

Fig. 5. Weibull strength analysis for ceramics in the AlN–SiC system (tensile tests).

origin, mirror, mist, and hackle as may be seen in Fig. 7(a). The fracture origins in AlN are typically large agglomerates surrounded by high porosity regions (Fig. 7(b)). Figure 8 presents a typical tensile fracture origin in 75%AlN–25%SiC specimens. The initiating flaw agglomerate appears to be highly porous with large grains of irregular morphology which are poorly bonded to the matrix (Fig. 8(b)). EDS results presented in Fig. 9 show a predominance of SiC in the porous region at the origin and an AlN rich region (the 'white area' in Fig. 9(a)) next to the flaw as compared to other regions of the surface. The Fe which is present at the failure origin, may play a role in this apparent segregation of SiC and AlN at the flaw. The fracture mirror in a typical 50%AlN–50%SiC failure origin appears to be smaller than in the case of AlN and 75%AlN–25%SiC (Fig. 6). The usual failure initiating flaw in the 50/50 solid solution alloy was an agglomerate composed of a mass of clustered grains with irregular morphology as shown in Fig. 10. Thus, it was sometimes difficult to locate the initiation of fracture. EDS indicated a lack of SiC at the agglomerate and the presence of pure AlN. The initiating flaw in a typical SiC specimen is also very difficult to locate. The failure initiating flaw appears to be a series of large interconnected pores adjacent to one or more large grains as may be seen in Fig. 11. A summary of the fractography of the four materials is presented in Table 3.

Table 2. Number of tested specimens, valid breaks and their locations

	AlN	*AlN–SiC (75%–25%)*	*AlN–SiC (50%–50%)*	*SiC*
No. specimens tested	15	14	9	15
No. valid breaks	11	10	9	13
Failure origin				
internal	5	6	7	8
near surface	3	2	2	5
indeterminate	1	2	0	0

Prediction of bend strength from tensile data

The four-point bend strength can be predicted from the tensile Weibull parameters by applying the standard Weibull scaling factor.[26]

$$\sigma_b = \sigma_t \left(\frac{\nu_t}{\nu_b}\right)^{\frac{1}{m}} \tag{1}$$

where

σ_t = the strength of the tensile specimens
ν_t = the effective volume of the tensile specimens
ν_b = the effective volume of the flexure specimens
m = Weibull modulus of the tensile specimens

The effective volume in the tensile specimen is the product of the cross-sectional area and the length of the gage section. For four-point bend specimen, the effective volume can be calculated using the following equation:[26]

$$\nu_{\text{eff.}} = \frac{bh}{2}\left(\frac{mL_2 + L_1}{(m+1)^2}\right) \tag{2}$$

where m is the tensile Weibull modulus, and the other parameters are defined in Fig. 4.

The characteristic flexural strength of the four materials were predicted from the tensile strength data. In addition, four-point bend tests of bend bars from the same batches of the four materials used to make the tensile rods were carried out and the Weibull distribution plotted as shown in Fig. 12. The characteristic strength, Weibull modulus,

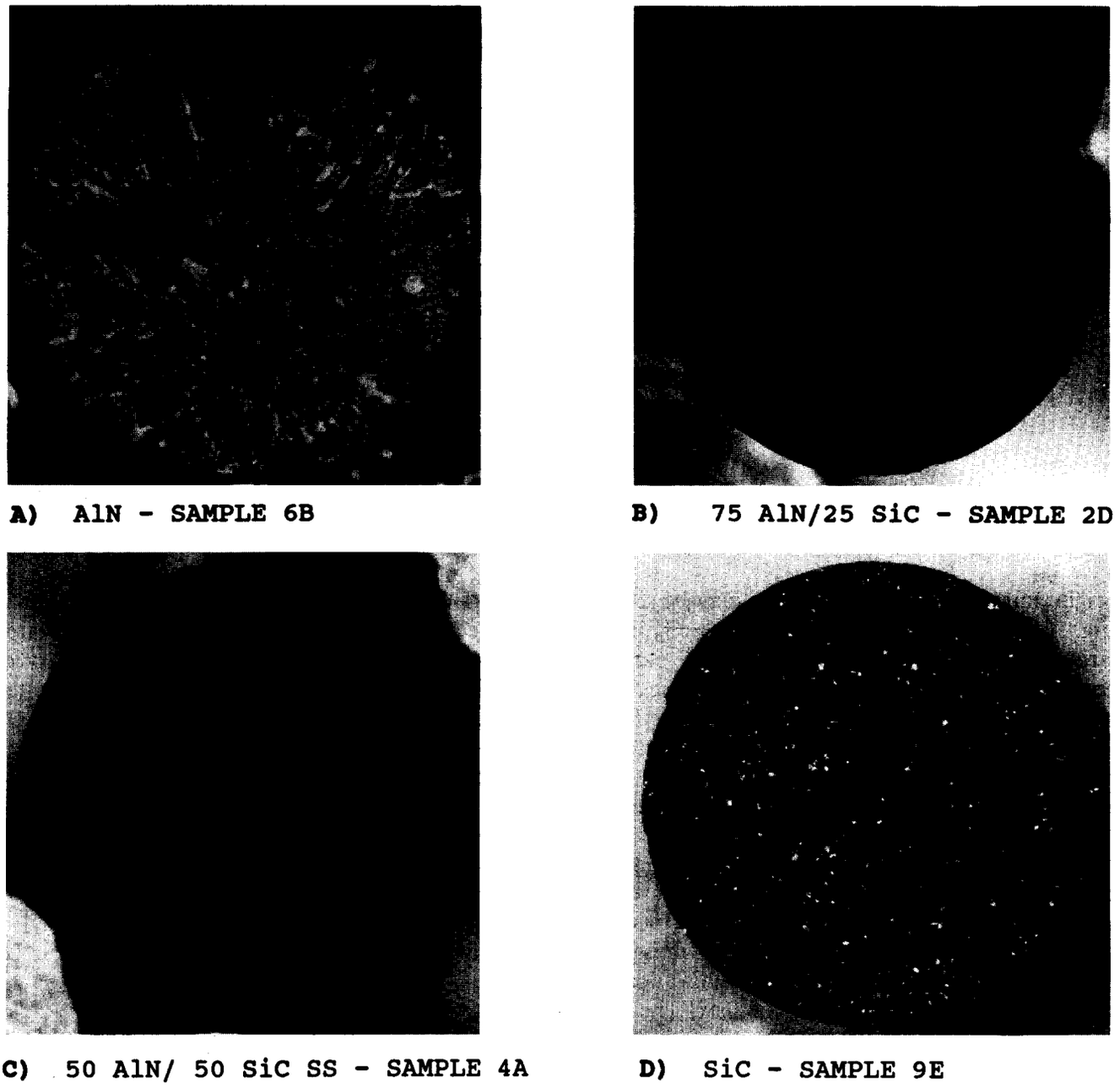

Fig. 6. Optical macro-fractography AlN–SiC system (sample diameter approximately 9 mm).

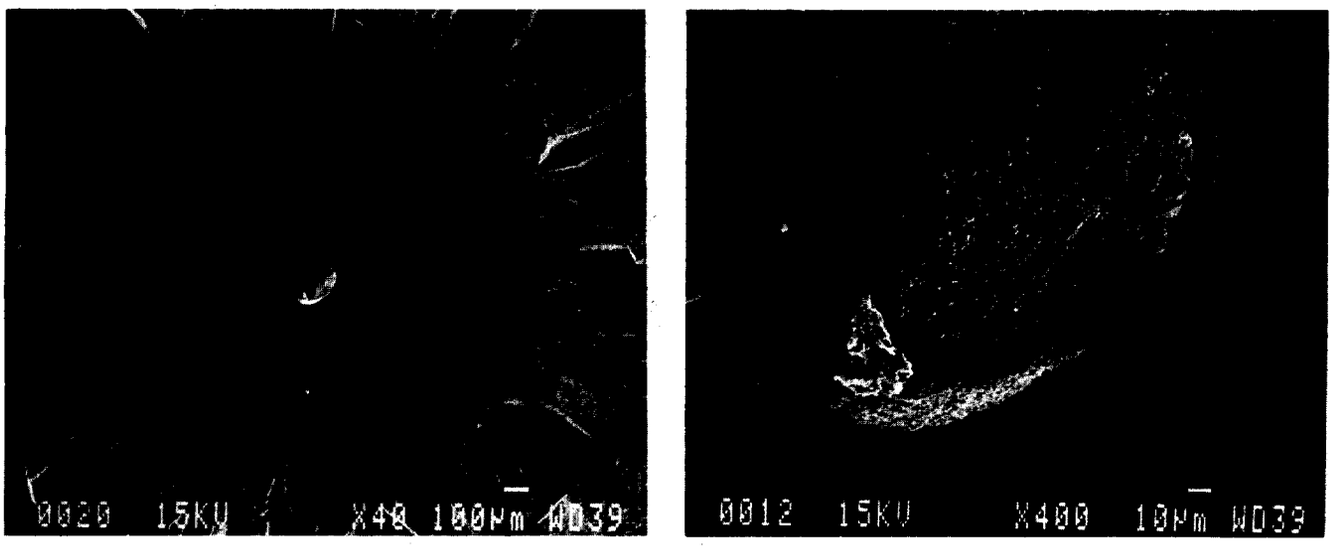

(A) (B)

Fig. 7. Typical tensile fracture origin in hot pressed AlN: (A) fracture mirror, (B) initiating flaw.

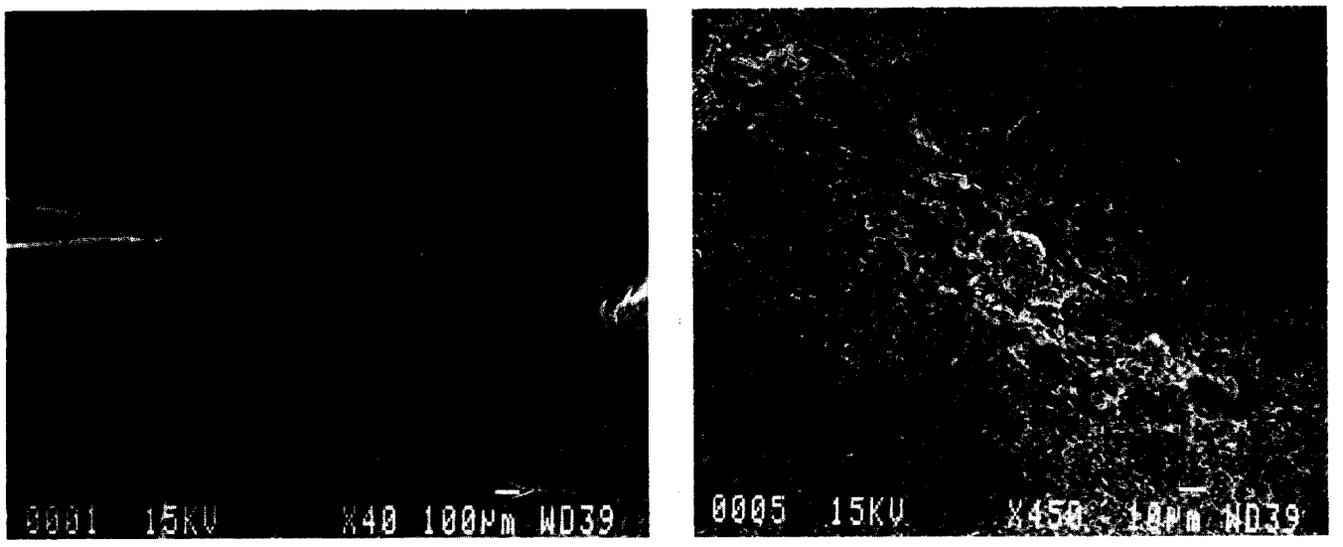

(a) (b)

Fig. 8. Typical tensile fracture origin in 75%AlN–25%SiC: (a) fracture mirror; (b) initiating flaw.

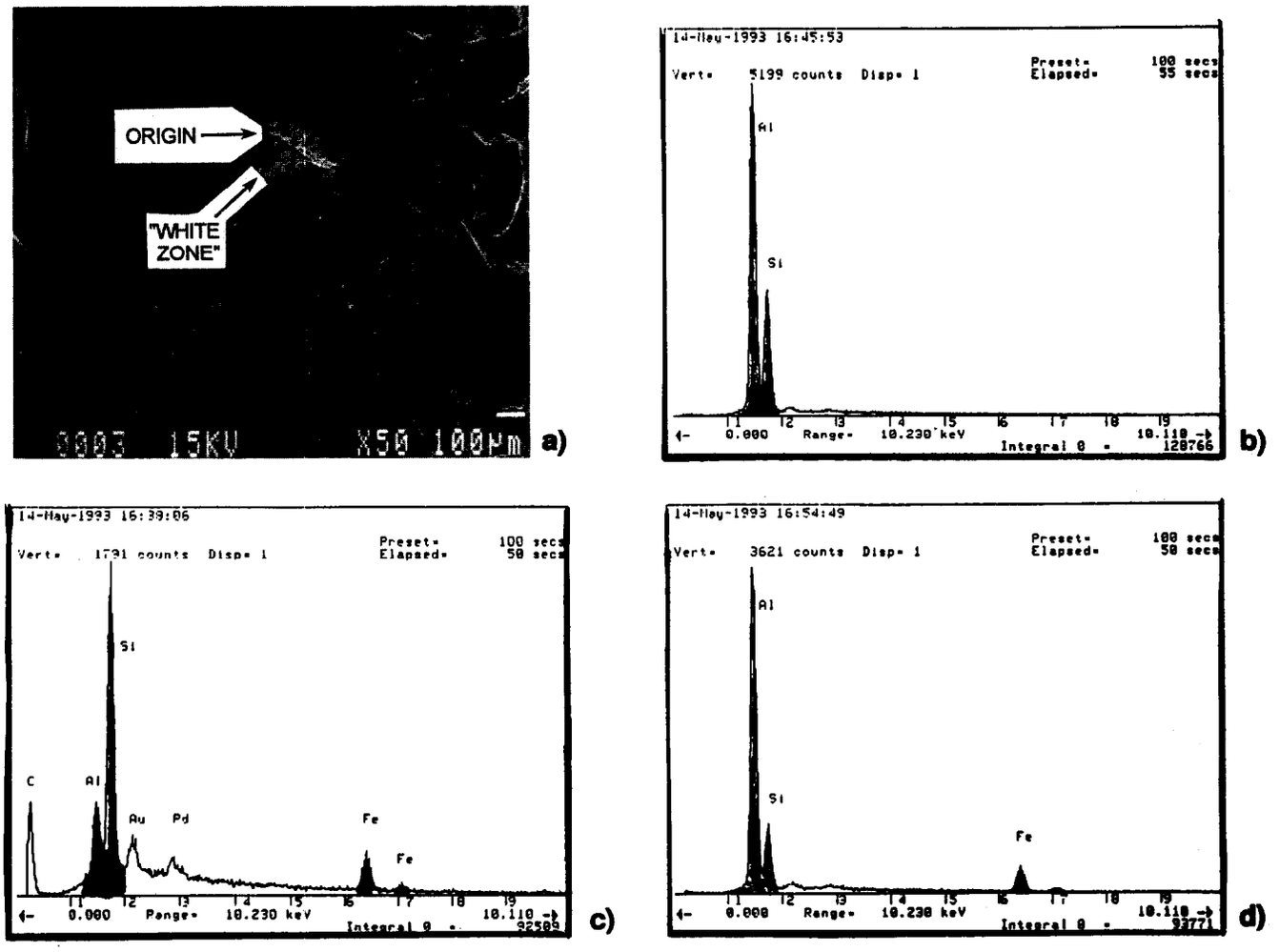

Fig. 9. EDS of failure including flaw in a 75%AlN–25%SiC composite: (a) SEM of initiating flaw and surrounding 'white zone', (b) Normal Si/Al peak height ratio far from origin of failure; (c) Si/Al peak height change indicating Al depletion in failure initiating flaw; (d) Si/Al peak height shift indicates Si depletion in the 'white zone'.

number of specimens, and the sum of the effective stressed volumes for each material are shown on the plot. The predicted and measured four-point bend strengths are compared in Table 4.

As can be seen from Table 4, the predicted flexural strength for the 75%AlN–25%SiC is in close agreement with the measured flexural strength. This is due to the fact that this material has a

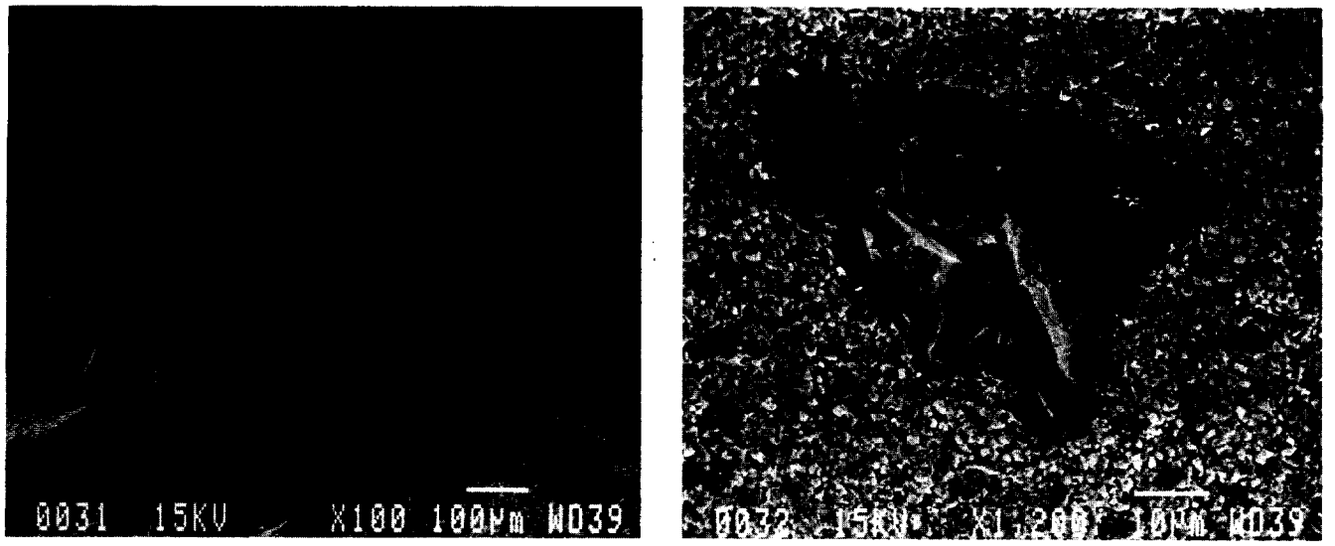

Fig. 10. Typical tensile fracture origin in 50%AlN–50%SiC.

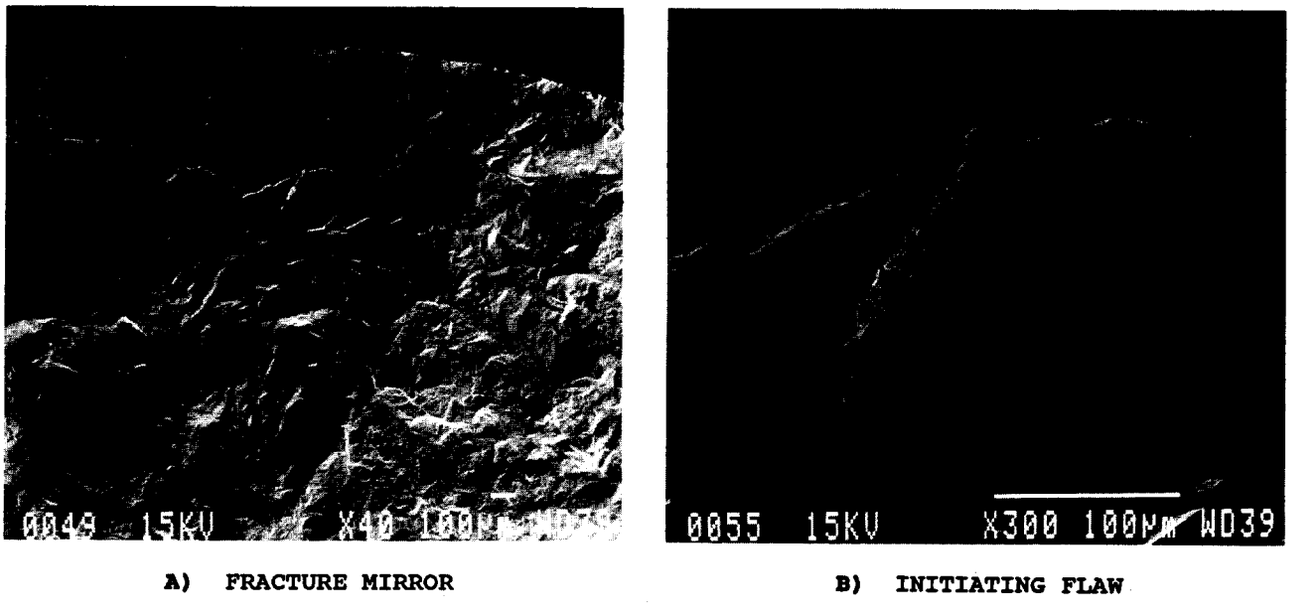

Fig. 11. Typical tensile fracture origin sintered SiC.

Table 3. Fractographical analysis of the ceramic specimens

Material	*Flaw*	*Flaw to matrix bonding characteristics*
AlN	AlN agglomerate circular morphology containing 'large grains' fully dense	Poorly bonded to matrix
75AlN–25SiC (particulate reinforced)	AlN deficient agglomerate irregular morphology 'large grains' highly porous AlN enriched 'white' area surrounding porous agglomerate	Poorly bonded to matrix
50AlN–50SiC (solid Solution)	AlN agglomerate irregular morphology 'large grains' fully dense	Well bonded to matrix
SiC	Large interconnected pores adjacent to large grain	N/A

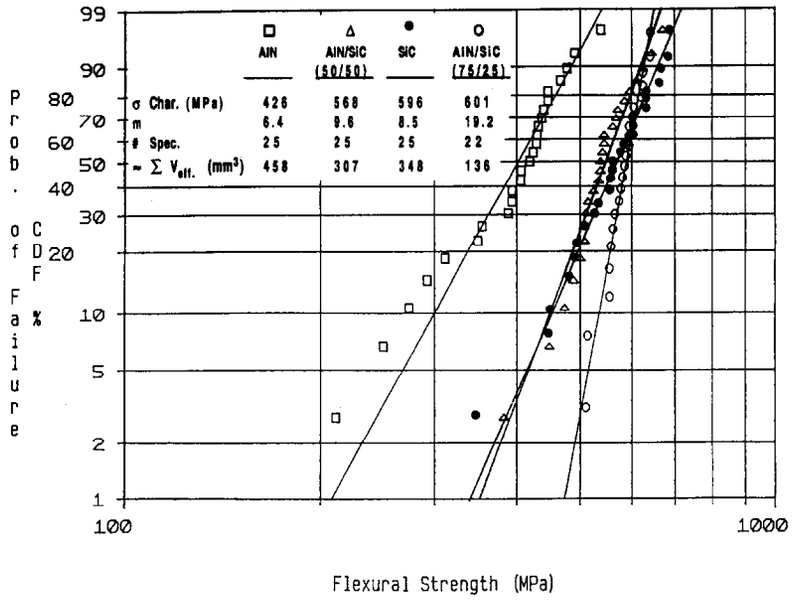

Fig. 12. Weibull strength analysis for ceramics in the AlN–SiC system (4-point bend tests).

Table 4. Predicted and measured flexural strength

Material	*Predicted* $\sigma_{char.}$ *(MPa)*	*Measured* $\sigma_{char.}$*(MPa)*	*Difference (%)*
75AlN/25SiC	605	601	–0·7
SiC	528	596	+11·4
50AlN/50SiC	450	568	+20·8
AlN	349	426	+18

Predictions based on $\sigma_{char.}$, $V_{eff.}$ and m obtained in tensile tests.

bimodal grain/phase structure and this bimodal structure gives rise to flaws that are uniformly dispersed throughout the matrix. The predicted bend strength values for the 50%AlN–50%SiC, AlN, and SiC vary by approximately 21, 18, and 11% of the measured values, respectively. This difference may be attributed to the difference in flaw populations initiating failure as compared to the 75%AlN–25%SiC material. In particular, the large AlN agglomerate which is encountered routinely in the tensile test with its large effective test volume, is likely to be only rarely encountered in bend bars. Identification of the AlN agglomerate as a common failure initiating fracture was obvious in studies of the tensile failures of AlN and 50%AlN–50%SiC, whereas, such a flaw was seen in only one of 25 bend bars. Similarly, the large grains with associated pores which are the failure origins in SiC, may be less frequently encountered in the small stressed volumes of the bend bars whereas, they are commonly encountered in the large tensile specimens. This graphically indicates the importance of obtaining fractographic analysis on tensile specimens as well as bend specimens, in order to be sure to identify all flaw populations.

Conclusions

This study has illustrated the following:

(1) Both the 75%AlN–25%SiC particulate reinforced and 50%AlN–50%SiC solid solution materials showed significantly increased strength as compared to pure AlN and SiC materials.

(2) While the nature of the failure initiating flaws varied for each of the four materials, agglomerates of AlN were common strength determining flaws in the pure AlN and 50%AlN–50%SiC solid solution. The prevalence of this flaw population was clearly evident in the tensile tests but not in the bend tests.

(3) The difference between predicted and measured flexural strength for the AlN, SiC, and 50%AlN–50%SiC materials may indicate that the flaw populations initiating failure differ. Because the tensile test interrogates a significantly larger stressed volume than does the bend test, the tensile test may well include flaw populations that are missed in conventional (10–30 specimens) bend testing. In such cases use of Weibull parameters obtained from tensile testing will tend to underpredict the fracture strength of the smaller component. Thus, the use of tensile data will yield a conservative design.

(4) Finally, the benefit of tensile tests in identifying failure initiating flaw populations was clearly demonstrated. Such information can provide useful feedback to materials' developers.

References

1. Katz, R. N., Opportunity and prospects for the application of structural ceramics. In *Treatise on Materials Science and Technology, 29: Structural Ceramics*. ed. J. B. Wachtman, Jr. Academic Press, Boston, MA, 1989, pp. 1–26.
2. Rafaniello, W., Plichta, M. R. & Virkar, A. V., Investigations of phase stability in the system SiC–AlN. *J. Am. Cer. Soc.*, **66**[6] (1983) 272–6.
3. Ruh, R., Zangvil, A. & Barlowe, J., Elastic properties of SiC, AlN and their solid solutions and particulate composites. *Bull Am. Soc.*, **64**[10] (1985) 1368–74.
4. Dutta, S., Strength distribution in commercial silicon carbide materials. *J. Am. Cer. Soc.*, **71**[11] (1988) C474–9.
5. Srinivasan, M., The Silicon Carbide family of structural ceramics. In *Treatise on Materials Science and Technology, 29: Structural Ceramics*, ed. J. B. Wachtman, Jr. Academic Press, Boston, MA, 1989, pp. 99–159.
6. Woodilla, D., Buonomo, M., Bar-On, I., Katz, R. N. & Whalen, T., Elevated-temperature behavior of high-strength Silicon Carbide. *J. Am. Cer. Soc.*, **76**[1] (1993) 249–52.
7. Boch, P., Glandus, J. C., Jarrige, J., Lecompte, J. P. & Mexmain, J., Sintering, oxidation, and mechanical properties of hot pressed Aluminum Nitride. *Ceramics International*, **8**[1] (1982) 34–40.
8. De With, G. & Hattu. N., Mechanical behavior of hot-pressed Aluminum Nitride ceramics. *Science of Ceramics*, **11** (1981) 489–94.
9. Skeele, F. P., Slavin, M. J. & Katz, R. N., Time–temperature dependence of strength in Aluminum Nitride. In *3rd International Symposium, Ceramic Materials & Components for Engines*, ed. V. J. Tenney, American Ceramic Society, 1989, pp. 710–8.
10. Katz, R. N., Wechsler, G., Toutanji, H., Friel, D., Leatherman, G. L., El-Korchi, T. & Rafaniello, W., Room temperature tensile strength of AlN. *Ceram. Eng. Sci. Proc.*, **14**(7–8). (1993) 282–91.
11. Ruh, R., & Zangvil, A., Composition and properties of hot-pressed SiC–AlN solid solutions. *J. Am. Cer. Soc.*, **65**[5] (1982) 260–5.
12. Landon, M. & Thevenot, F., The SiC–AlN system: Influence of elaboration routes on the solid solution formation and its mechanical properties. *Ceramics International*, **17**[1] (1991) 97–100.
13. Miura, M., Yogo, T. & Hirano, S., Microstructure and mechanical properties of SiC–AlN ceramics after phase separation treatment. *J. Cer. Soc. Jpn.*, **101**[7] (1993) 793–99.
14. Miura, M., Yogo, T. & Hirano, S., Mechanical and thermal properties of SiC–AlN ceramics with modulated texture. *J. Cer. Soc. Jpn.*, **101**[11] (1993) 1281–6.
15. Mariano, S. A., Friel, D. & Bar-On, I., Evaluated temperature mechanical properties of SiC–AlN particulate composites, *Ceram. Eng. Proc.*, **14**[9–10] (1993) 1077–88.
16. Rafaniello, W., Development of Aluminum Nitride: a new low-cost armor, Final Report U.S. Army Research Office, Contract Number DAAL03-88-C-001 2 Dec. 1992.
17. Flexural strength of high performance ceramics at ambient temperature, MIL-STD-1942 (MR), Army Materials Technology Laboratory, Watertown, MA, Nov. 1983.
18. Rafaniello, W., unpublished research, Dow Chemical Co.
19. Baratta, F. I. & Driscoll, G. W., A new axial tension tester for brittle materials, Army Materials and Mechanics Research Center, AMMRC TR 69-02, Watertown, MA, 1968.
20. Driscoll, G. W. & Baratta, F. I., Modifications to an axial tension tester for brittle materials, Army Materials and Mechanics Research Center, AMMRC PTR 71-3, Watertown, MA, 1971.
21. Hermansson, L., Adlerborn, J. & Burstrom, M., Tensile testing of ceramic materials—A new approach. In *High Tech Ceramics*, ed. P. Vincenzini, Elsevier Science Publishers B. V., Amsterdam, 1987, pp. 1161–8.
22. ASEA CERAMA AB, Introduction and Operation Manual for ASCERA Hydraulic Tensile Testing, Robertsfors, Sweden, 1988.
23. Lucas, H. P., Direct tensile testing of brittle materials, Master Thesis, (1991), Worcester Polytechnic Institute, Worcester, MA.
24. Toutanji, H. A., El-Korchi, T., Leatherman, G. L. & Katz, R. N., Tensile strength of Carbon fiber reinforced cement composites. In *Fiber Reinforced Cementitious Composites*, Mat. Res. Soc. Symp. Proc., **245**, 1992, pp. 359–64.
25. Toutanji, H. A., The development of a cementitious composites axial tensile technique and its application to Carbon fiber reinforced cementitious composites, Ph.D. Thesis, Worcester Polytechnic Institute, Worcester, MA, 1992.
26. McLean, A. F. & Hartsock, D. L., Design with structural ceramics. In *Treatise on Materials Science and Technology, 29: Structural Ceramics*, ed. J. B. Wachtman, Academic Press, Inc., 1989 pp. 27–95.